

Diffusive oscillators capture the pulsating states of deformable particles

Alessandro Manacorda^{1,2,*} and Étienne Fodor^{2,†}

¹*CNR Institute of Complex Systems, Uos Sapienza, Piazzale A. Moro 5, 00185 Rome, Italy*

²*Department of Physics and Materials Science, University of Luxembourg, L-1511 Luxembourg, Luxembourg*

(Received 19 December 2023; revised 16 December 2024; accepted 22 April 2025; published 12 May 2025)

We study a model of diffusive oscillators whose internal states are subject to a periodic drive. These models are inspired by the dynamics of deformable particles with pulsating sizes, where repulsion leads to arrest the internal pulsation at high density. We reveal that, despite the absence of any repulsion between the diffusive oscillators, our model still captures the emergence of dynamical arrest. We demonstrate that arrest here stems from the discrete nature of internal states, which enforces an effective energy landscape analogous to that of deformable particles. Moreover, we show that the competition between arrest and synchronization promotes spiral waves reminiscent of the pulsating states of deformable particles. Using analytical coarse graining, we derive and compare the collective dynamics of diffusive oscillators with that of deformable particles. This comparison leads to rationalizing the emergence of spirals in terms of a rotational invariance at the coarse-grained level, and to elucidating the role of hydrodynamic fluctuations.

DOI: [10.1103/PhysRevE.111.L053401](https://doi.org/10.1103/PhysRevE.111.L053401)

Introduction. Active matter encompasses systems where a constant energy injection at the particle level leads to collective dynamics far from equilibrium, as is the case for many chemical, biological, and robotic systems [1–4]. In the last decades, most studies of active matter have focused on the role of self-propulsion, i.e., the ability of each particle to independently undergo directed motion. This paradigm has led to the theoretical understanding of several kinds of collective dynamics, which have no counterpart in equilibrium systems [5,6].

The energy injection in complex units need not result only in a self-propulsion mechanism. An important example is the case of deformable particles [7]. Indeed, complex aggregates such as macromolecules or living cells can change their shape due to internal activity [8], which leads to the spontaneous propagation of contraction waves in dense tissues. Such a wave propagation plays a crucial role in morphogenesis [9–14], uterine contraction [15,16], and cardiac arrhythmogenesis [17,18].

Vertex models are popular to capture the behavior of dense active systems such as biological tissues [19]. They typically consider self-propulsion as the only active component and investigate how it affects the rigidity transition [20,21]. Yet, when dense tissues behave like solids, it is questionable whether self-propulsion should be the key ingredient. Other models have considered dense assemblies of deformable particles [22–30], where energy injection occurs through the sustained oscillation of individual sizes. With a Kuramoto-like synchronization [31,32] of particle sizes, contraction waves spontaneously emerge [26,27,33], which are reminiscent of those reported in biological systems [13,17].

Contraction waves in deformable active particles stem from the competition between synchronization and steric

repulsion [27,33]. The former favors a global cycling of particle sizes. The latter favors some specific deformations, which is analogous to enforcing an external potential through which particle sizes are driven [Fig. 1(a)]. At high density, local minima are deep enough to trap the particle size and thus promote an arrested state. Here, arrest refers to the hampering of size cycling, whereas it corresponds to the hampering of particle displacement within the rigidity transition of Ref. [20].

Interestingly, there are alternative mechanisms for arrest and synchronization beyond steric repulsion and Kuramoto-like interactions. This is a motivation for exploring whether these alternatives lead to a phenomenology similar to that of deformable active particles. Indeed, one may wonder whether the arrest-synchronization competition is actually a

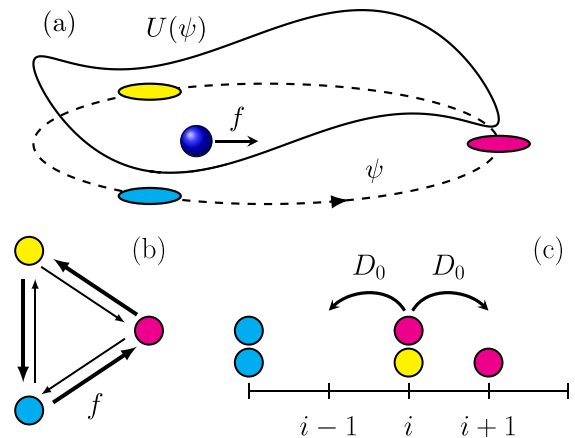


FIG. 1. (a) The collective dynamics of deformable particles maps into a continuous oscillator ψ evolving in a potential U and subject to a drive f (Ref. [34], Sec. S1.D). (b) The internal dynamics of our discrete oscillator follows some transitions biased by the drive f without any potential. (c) Our oscillators freely diffuse at a rate D_0 without any volume exclusion.

*Contact author: alessandro.manacorda@isc.cnr.it

†Contact author: etienne.fodor@uni.lu

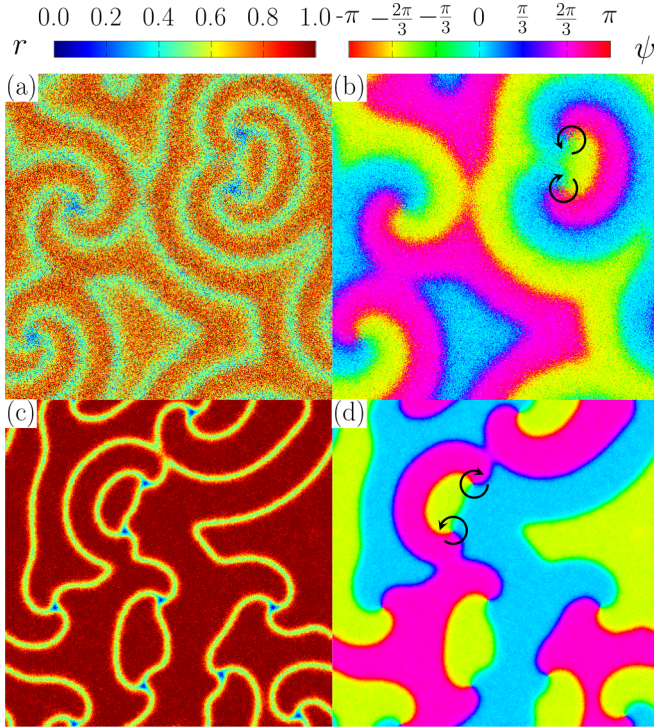


FIG. 2. The amplitude r and the phase ψ of synchronization [Eq. (5)] reveal the coexistence of ordered domains in (a)–(b) microscopic dynamics [Eq. (1)], and (c)–(d) hydrodynamics [Eq. (8)]. Rotating defects appear at the meeting point of domain interfaces, forming spiral waves with a threefold symmetry. (a) $(L, f, \varepsilon, D_0, \rho_0) = (512, 1.25, 2.5, 10^3, 10)$, and (b) $(L, f, \varepsilon, D, \rho_0) = (512, 0.5, 2.5, 100, 10)$.

generic scenario for pattern formation. If so, it encourages one to search for any hydrodynamic invariance and/or broken symmetry, which might stand out as a hallmark of this competition.

In this Letter, we study a diffusive oscillator model (DOM) (Fig. 1) featuring spiral waves rotating around defects (Fig. 2). We reveal that the discreteness of internal states is key to arresting the dynamics, which, in combination with synchronization and drive, generically yields wave propagation. Internal states can here be regarded as representing the local minima of an external potential [Fig. 1(a)], by analogy with the case of deformable particles [27,33]. Through analytical coarse graining, we map our DOM into a specific form of the complex Ginzburg-Landau equation (CGLE) [35], which breaks the continuous rotational invariance, while maintaining a discrete rotational invariance. We argue that such an invariance not only signals the emergence of arrest, but also constrains the features of the waves at the hydrodynamic and microscopic levels. Moreover, we reveal that hydrodynamic noise is essential to forming patterns, whereas density fluctuations are irrelevant.

Overall, our results demonstrate that the arrest-synchronization competition, present in our DOM and in deformable particles [27,33], is a generic route for forming patterns, which are distinct from those of standard reaction-diffusion systems (RDS) [36–38].

Diffusive oscillator model. We consider N oscillators in $V = L^d$ sites of a hypercubic d -dimensional lattice, with global number density $\rho_0 = N/V$, without any excluded volume. Each site contains an arbitrarily large number of oscillators. Each oscillator has an internal state, labeled by a discrete index $a \in \{1, \dots, q\}$, as a proxy to mimic the internal phase of deformable particles [22–27,33]. The crucial difference is that such states now feature a discrete symmetry. In what follows, we focus on the case $q = 3$, which is the minimum number of states to accommodate a current, and $d = 2$. The system configuration $\{n_{\mathbf{j},a}\}$ is then given by the number of oscillators for each state a and site \mathbf{j} .

At every time step dt/N , an oscillator with state a can either jump to a neighboring site with probability $D_0 dt$, or switch to state b with probability $W_{ba} dt$ [Figs. 1(b), 1(c)]:

$$W_{ba} = \exp \left[-f_{ba} + \frac{\varepsilon}{\rho_{\mathbf{j}}} (n_{\mathbf{j},b} - n_{\mathbf{j},a}) \right]. \quad (1)$$

The first term in the exponent of Eq. (1) is defined by $f_{ab} = \pm f$ when $a - b = \pm 1 \pmod{3}$, and $f_{ab} = 0$ otherwise. This drive mimics the pulsation of deformable particles [22–27,33]. Following previous examples of driven and active lattice dynamics [39–46], the second term accounts for a synchronizing Potts-like [47] interaction with strength ε , where $\rho_{\mathbf{j}} = \sum_a n_{\mathbf{j},a}$ is the local density at site \mathbf{j} . This term favors transition towards the state with the highest number of oscillators locally.

While interactions between oscillators are fully connected onsite, different sites exchange information only via diffusion. At small D_0 , many transitions of internal states occur in between two rare jumps of sites. At large D_0 , jumps are so frequent that now all oscillators are effectively interacting in between two state transitions. In both cases, patterns cannot emerge, and the system can be described solely in terms of the onsite dynamics [48,49].

Breakdown of rotational invariance: Analogy with deformable particles. In the absence of diffusion ($D_0 = 0$), the evolution of the on-site occupation numbers n_a can be studied in terms of the collective complex variable

$$A(t) = \frac{1}{\rho_0} \sum_{a=1}^3 e^{\frac{2\pi i}{3} a} n_a(t) \equiv r(t) e^{i\psi(t)}. \quad (2)$$

Coarse graining the microscopic dynamics, and expanding to the lowest orders in A , we get ([34], Secs. S1.A–B)

$$\dot{A} = c_1 A + c_2 A^{*2} + c_3 |A|^2 A \equiv \mathcal{L}(A), \quad (3)$$

where $*$ refers to complex conjugation, and (c_1, c_2, c_3) are complex coefficients fixed by (f, ε) ([34], Sec. S1.B). In the regime of large ρ_0 , fluctuations become irrelevant. The A^{*2} term in Eq. (3) breaks the continuous symmetry $A \rightarrow A e^{i\phi}$, in contrast with the standard Stuart-Landau oscillator [50]. Yet, this term preserves the discrete symmetry $A \rightarrow A e^{\frac{2\pi i}{3} k}$ (k integer). To the third order in A , Eq. (3) actually contains all the terms compatible with this rotational symmetry.

From the dynamics in Eq. (3), it follows that there are three stable phases [48,49] (Fig. 3): (i) a disordered phase at small ε , where oscillators are uniformly distributed in the three states, with symmetric fixed point $n_a = \rho_0/3$, and $|A|$

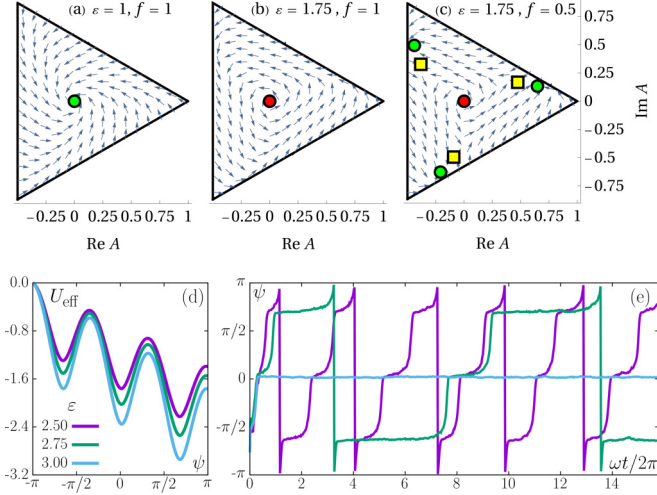


FIG. 3. Stream plots of the collective variable A [Eq. (3)] for (a) disorder, (b) cycles, and (c) arrest, with stable fixed points (green circles), unstable fixed points (red circles), and saddles (yellow squares). (d) Effective landscape U_{eff} of the collective phase ψ [Eq. (4)] with $f = 0.1$. (e) Stochastic trajectories of ψ measured in the onsite dynamics [Eq. (1)]. As ε increases, phase oscillations slow down, and eventually reach arrest. $(N, f) = (10^3, 2)$ and ε as in (d). The natural pulsation reads $\omega = \sqrt{3} \sinh f$ ([34], Sec. S1.B).

vanishes at large ρ_0 ; (ii) a cycling phase at intermediate ε , where oscillators collectively undergo periodic transitions between states; (iii) an arrested phase at large ε , with three fixed points invariant under the cyclic permutations $A \rightarrow A e^{\frac{2\pi i}{3}k}$.

The breakdown of the continuous symmetry $A \rightarrow A e^{i\phi}$ ensures the existence of arrest, while the discrete symmetry $A \rightarrow A e^{\frac{2\pi i}{3}k}$ enforces that the arrested phase is actually degenerate. Note that, in the microscopic model [Eq. (1)], transitions between states can be regarded as unimolecular reactions, in contrast with some models of multimolecular RDS [51,52], and the total number of oscillators is conserved. These features lead to stabilizing disorder at small ε , and ensure that arrest at large ε is not an absorbing phase.

In the arrested phase, the discrete nature of the internal states enforces that the collective phase ψ is subject to the effective landscape U_{eff} ([34], Sec. S1.C):

$$\dot{\psi} = -dU_{\text{eff}}/d\psi. \quad (4)$$

Remarkably, U_{eff} features a series of local periodic minima whose depth increases with ε [Fig. 3(d)], which can be rationalized in simple terms. At large ε , while continuous oscillators [31] synchronously cycle without any cost, the collective cycling of our discrete oscillators [Eq. (1)] entails some periodic desynchronizations: the minima in U_{eff} describe the cost of such desynchronizations. As ε increases, transitions between minima are less favored, so that our oscillators spend more time in a given state before cycling to the next one. Above a critical ε , this effect completely counteracts the drive, breaking down the periodicity of oscillations, and eventually stabilizing arrest [Fig. 3(e)].

Interestingly, a similar phase trapping has been reported in deformable particles [26,27,33]. Here, repulsion between particles is equivalent to an external potential constraining the

deformation statistics [Fig. 1(a)]. At the collective level, such a constraint can be recapitulated in terms of a landscape with periodic minima ([34], Sec. S1.D), qualitatively analogous to U_{eff} [Fig. 3(d)]. In that respect, our DOM captures the same phenomenology, with identical collective states (disorder, arrest, cycles) as that of pulsating deformable particles.

In short, arrest emerges in our DOM solely due to the discreteness of internal states. As a result, our DOM entails a competition between arrest and synchronization despite the absence of any repulsion, in contrast with deformable particles [26,27,33]. This competition opens the door to the emergence of dynamical patterns in spatially extended systems.

Spiral waves rotate around defects. In the presence of diffusion ($D_0 > 0$), the displacement of oscillators follows a free dynamics, independently of any interaction, so that the density profile is always homogeneous. Yet, the spatial distribution of the oscillator states may not remain homogeneous. Indeed, even when oscillators are synchronized on site, they might not be synchronized between sites, so that the system can potentially accommodate spatial instabilities.

To study the emergence of dynamical patterns, we introduce the local complex variable

$$A_j(t) = \frac{1}{\rho_j(t)} \sum_{a=1}^3 e^{\frac{2\pi i}{3}a} n_{j,a}(t) \equiv r_j(t) e^{i\psi_j(t)}. \quad (5)$$

When all oscillators are cycling in synchrony, the amplitude $r_j \approx 1$ and the phase ψ_j are homogeneous. The period of ψ_j increases with ε , and eventually diverges. Before diverging, it undergoes large temporal fluctuations, which may desynchronize nearby sites, thus promoting spatial fluctuations of ψ_j . At large D_0 , spatial fluctuations are suppressed by the rapid displacement of oscillators in the system. Instead, at moderate D_0 , such fluctuations can potentially build up into a large-scale instability.

Instabilities can lead to the spatial coexistence of three cycling domains where $r_j \equiv r_{j,c} \approx 1$. Interfaces between domains have a finite width where $r_{j,c} > r_j > 0$. The meeting points of interfaces are given by defects where $r_j \approx 0$. Since all domains cycle at the same frequency, defects effectively rotate, thus forming spiral waves with a threefold symmetry [Figs. 2(a)–2(b)]. Defects connected by the same interface rotate in opposite directions, and can annihilate by pairs when colliding. Higher D_0 increases the domain sizes and interface widths, thus reducing the number of defects. Higher ε reduces the interface widths and increases $r_{j,c}$ [Fig. 4(a)].

Remarkably, we do not observe any states with turbulent waves, in contrast with the case of continuously deformable particles [27]. Such a turbulence stems in Ref. [27] from excitations of the homogeneous arrested phase, which promote some localized, aperiodic cyclings. The discrete symmetry of our DOM, which entails three arrested states, prevents such events by trapping the phase before it completes one cycle. Therefore, waves in our DOM spontaneously organize into steady spirals with threefold symmetry. Note that the merging of defects can actually also stabilize planar waves. Besides, when initially ordered, the system can also accommodate circular waves without any defect ([34], Sec. S2.A).

Phase boundaries and transitions. In addition to the phase with waves, we also observe the emergence of three homoge-

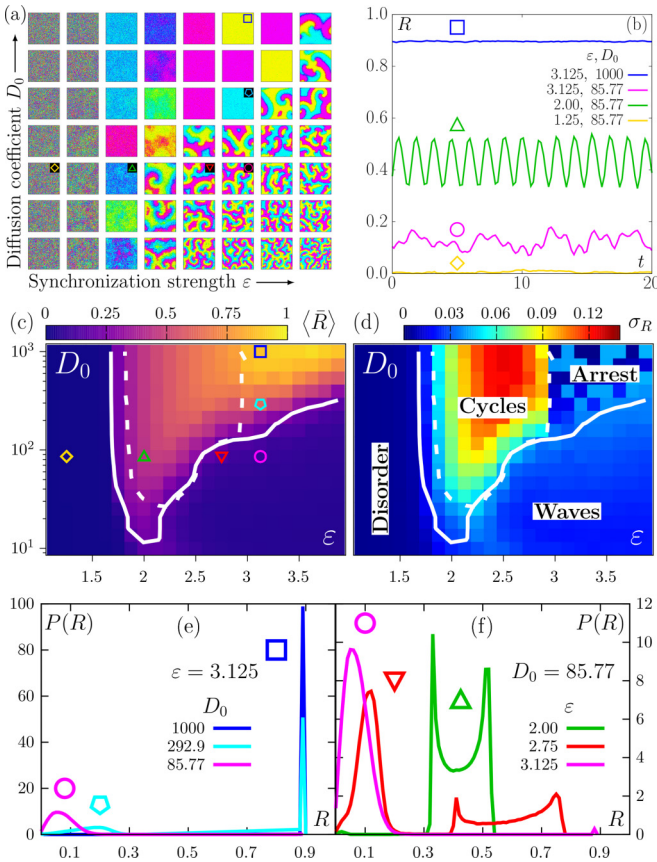


FIG. 4. (a) Snapshots of the local phase ψ_j [Eq. (5), color code in Fig. 2]. (b) Trajectories of the synchronization parameter $R(t)$ [Eq. (6)]. (c) The averaged parameter $\langle \bar{R} \rangle$ and (d) its standard deviation σ_R [Eq. (7)] lead to guidelines delineating boundaries between four phases. The solid and dashed lines correspond respectively to $\langle \bar{R} \rangle = 0.2$ and $\sigma_R = 0.045$. Symbols refer to the parameter values taken for (a)–(b) and (e)–(f). (e), (f) Distribution of R for various phases (1024 realizations). The arrested-wave and cycling-wave transitions both display metastability. $(L, \rho_0) = (128, 10)$, and $f = \varepsilon/2$.

neous phases (disorder, cycles, arrest) analogous to the on-site case. To quantitatively distinguish these phases, we introduce the synchronization parameter

$$R(t) = \frac{1}{N} \left| \sum_{j,a} e^{\frac{2\pi i}{3} a} n_{j,a}(t) \right|. \quad (6)$$

The trajectories of $R(t)$ allow us to identify four scenarios [Figs. 4(a), 4(b)]: (i) a disordered phase at small ε [$R(t) \approx 0$, yellow line]; (ii) a cycling phase at intermediate ε and large D_0 [oscillating $R(t)$, green line]; (iii) an arrested phase at large ε and large D_0 [$R(t) \lesssim 1$, blue line]; (iv) spiral waves at large ε and intermediate D_0 [$R(t)$ strongly fluctuates, pink line].

To delineate phase boundaries, we consider the time-averaged \bar{R} and the variance σ_R^2 of $R(t)$ [Eq. (6)]:

$$\bar{R} = \int_{t_0}^{t_0+t} \frac{R(u) du}{t}, \quad \sigma_R^2 = \int_{t_0}^{t_0+t} \frac{\langle [R(u) - \bar{R}]^2 \rangle du}{t}, \quad (7)$$

where $\langle \cdot \rangle$ is an average over realizations. $\langle \bar{R} \rangle$ is clearly smaller in the disordered and wave phases (without global

synchronization) than in the cycling and arrested phases (with global synchronization) [Fig. 4(c)]. The variance σ_R is higher in the cycling phase than in all others [Fig. 4(d)]. Indeed, $R(t)$ strongly oscillates in this phase [Fig. 4(b)] due to periodic desynchronization. Overall, $\langle \bar{R} \rangle$ and σ_R yield the phase boundaries in Figs. 4(c)–4(d).

We examine how the distribution $P(R)$ varies across transitions. Deep in the wave and arrested phases (pink and dark blue lines), $P(R)$ has a single peak, respectively at small and large R . Deep in the cycling phase [green line], $P(R)$ is nonzero for a finite domain of R and peaks at its boundaries, due to the oscillations of $R(t)$. Going from waves to arrest, $P(R)$ becomes bimodal, thus signaling metastability [Fig. 4(e)]. Similarly, going from waves to cycling, $P(R)$ is now nonzero in two separate domains, due to the coexistence between the two dynamical states [Fig. 4(f)]. In short, both the arrest-wave and cycling-wave transitions feature a metastable regime.

Role of hydrodynamic fluctuations. Although spiral waves have already been reported in many RDS, one may wonder how our patterns [Figs. 2(a)–2(b)] actually differ from standard instabilities present, for instance, in the CGLE [35]. To address this question, we coarse grain our DOM in terms of $A_j(t) \rightarrow \mathcal{A}(\mathbf{x}, t)$ and $\rho_j(t) \rightarrow \rho(\mathbf{x}, t)$ in the continuum limit, and expand to the lowest orders in \mathcal{A} ([34], Sec. S1.B):

$$\partial_t \mathcal{A} = D \nabla^2 \mathcal{A} + \mathcal{L}(\mathcal{A}) + \Lambda, \quad (8)$$

where \mathcal{L} is defined in Eq. (3), and $D \propto D_0$ is the macroscopic diffusion coefficient. Neglecting the fluctuations of the coarse-grained density $\rho(\mathbf{x}, t)$, we deduce that it obeys the simple diffusion equation ($\partial_t \rho = D \nabla^2 \rho$) independently of \mathcal{A} , and relaxes to the homogeneous profile $\rho = \rho_0$. Thus, we approximate Λ as an additive zero-mean Gaussian white noise with correlations proportional to $1/\rho_0$ ([34], Sec. S1.B).

The degeneracy of the arrested state directly affects the shape of the hydrodynamic patterns. Indeed, Eq. (8) entails an instability promoting the spatial coexistence of cycling domains. Rotating defects with threefold symmetry spontaneously form where interfaces meet [Figs. 2(c)–2(d)], yielding the same spiral waves as in our DOM [Figs. 2(a)–2(b)]. Remarkably, in the absence of noise ($\Lambda = 0$), the homogeneous states are always stable ([34], Sec. S1.B). In other words, while density fluctuations can be safely neglected, the fluctuations in the hydrodynamics of \mathcal{A} are essential to capture patterns, as in Ref. [27].

In short, our coarse-graining shows that the hydrodynamics of our DOM is distinct from the standard CGLE [35], so that our DOM clearly differs from standard RDS. In practice, adding to the standard CGLE the lowest-order nonlinearities, compatible with the discrete symmetry, suffices to reproduce the specific shape of spirals observed in our DOM.

Discussion. Our DOM with discrete symmetry entails spiral waves stemming from the competition between arrest and synchronization (Fig. 2). The key idea is that discrete states enforce an effective landscape [Fig. 3(d)] equivalent to the case of deformable particles with repulsive interactions ([34], Sec. S1.D) [27,33]. Discreteness of states here suffices to promote arrest, thus providing a mechanism distinct from that at play in Refs. [27,33]. Therefore, our results show

that the arrest-synchronization scenario for pattern formation extends to a broad class of models with discrete symmetry. Waves are shaped by the discrete rotational invariance at the hydrodynamic level, which distinguishes them from the patterns of other RDS [36–38]. Remarkably, pattern formation occurs in presence of a single, real-valued diffusion coefficient D , in contrast with standard pattern formation in CGLE [35]. The stability analysis clarifies that fluctuations of the complex field are crucial to yield patterns, whereas density fluctuations are irrelevant.

Our work paves the way to examining the interplay between discrete symmetry and pattern formation for arbitrary q . Indeed, we expect that the three homogeneous phases (disorder, cycles, arrest) are robust beyond $q = 3$. To study patterns, one can use a top-down approach postulating the hydrodynamics by identifying the terms which obey the discrete symmetry $\mathcal{A} \rightarrow \mathcal{A}e^{\frac{2\pi i}{q}k}$. As in our coarse graining ([34], Sec. S1), one can also derive the hydrodynamic coefficients in terms of the microscopic parameters. It is tempting to speculate that, depending on the parity of q , such a hydrodynamic study could lead to identifying generic properties of defect dynamics [53,54]. The interplay between arrest and synchronization also plays a crucial role in other active models with phase trapping [46,55–58]; exploring the connections between these models represents a theoretical challenge for a unified picture of pattern formation in active matter.

The discrete symmetry of our DOM seems to preclude a defect turbulence, at variance with the standard CGLE [35] and its recent generalization [27]. To capture such a turbulence, one could introduce energy levels, which maintain the discrete nature of our DOM while breaking its symmetry. The arrested phase would no longer be degenerate, thus opening the door to local excitations nucleating defects from a homogeneous phase, as reported in Refs. [27,33]. In this context, it would be interesting to explore how density fluctuations affect the defect nucleation at the hydrodynamic and microscopic levels [59]. Finally, our DOM can be straightforwardly adapted to account for thermodynamic consistency [60], allowing one to study the energetics of the corresponding patterns [61–63].

Acknowledgments. We acknowledge fruitful discussions with L. K. Davis, M. Esposito, J. Meihbom, and Y. Zhang. This project has received funding from the European Union’s Horizon Europe research and innovation programme under the Marie Skłodowska-Curie Grant Agreement No. 101056825 (NewGenActive), and from the Luxembourg National Research Fund (FNR), Grant reference No. 14389168. A.M. acknowledges financial support from the project MOCA funded by MUR PRIN2022 Grant No. 2022HNW5YL.

Data availability. The data that support the findings of this article are openly available [64].

-
- [1] T. Vicsek and A. Zafeiris, Collective motion, *Phys. Rep.* **517**, 71 (2012).
- [2] M. C. Marchetti, J. F. Joanny, S. Ramaswamy, T. B. Liverpool, J. Prost, M. Rao, and R. A. Simha, Hydrodynamics of soft active matter, *Rev. Mod. Phys.* **85**, 1143 (2013).
- [3] C. Bechinger, R. Di Leonardo, H. Löwen, C. Reichardt, G. Volpe, and G. Volpe, Active particles in complex and crowded environments, *Rev. Mod. Phys.* **88**, 045006 (2016).
- [4] É. Fodor and M. C. Marchetti, The statistical physics of active matter: From self-catalytic colloids to living cells, *Physica A* **504**, 106 (2018).
- [5] M. E. Cates and J. Tailleur, Motility-induced phase separation, *Annu. Rev. Condens. Matter Phys.* **6**, 219 (2015).
- [6] H. Chaté, Dry aligning dilute active matter, *Annu. Rev. Condens. Matter Phys.* **11**, 189 (2020).
- [7] M. L. Manning, Essay: Collections of deformable particles present exciting challenges for soft matter and biological physics, *Phys. Rev. Lett.* **130**, 130002 (2023).
- [8] S. Zehnder, M. Suaris, M. Bellaire, and T. Angelini, Cell volume fluctuations in MDCK monolayers, *Biophys. J.* **108**, 247 (2015).
- [9] J. Solon, A. Kaya-Çopur, J. Colombelli, and D. Brunner, Pulsed forces timed by a Ratchet-like mechanism drive directed tissue movement during dorsal closure, *Cell* **137**, 1331 (2009).
- [10] A. C. Martin, M. Kaschube, and E. F. Wieschaus, Pulsed contractions of an actin–myosin network drive apical constriction, *Nature (London)* **457**, 495 (2009).
- [11] G. B. Blanchard, S. Murugesu, R. J. Adams, A. Martinez-Arias, and N. Gorfinkiel, Cytoskeletal dynamics and supracellular organisation of cell shape fluctuations during dorsal closure, *Development* **137**, 2743 (2010).
- [12] K. Kruse and D. Rivelino, Chapter three - spontaneous mechanical oscillations: Implications for developing organisms, in *Forces and Tension in Development*, edited by M. Labouesse, Current Topics in Developmental Biology Vol. 95 (Academic Press, New York, 2011), pp. 67–91.
- [13] X. Serra-Picamal, V. Conte, R. Vincent, E. Anon, D. T. Tambe, E. Bazellieres, J. P. Butler, J. J. Fredberg, and X. Trepat, Mechanical waves during tissue expansion, *Nat. Phys.* **8**, 628 (2012).
- [14] C.-P. Heisenberg and Y. Bellaïche, Forces in tissue morphogenesis and patterning, *Cell* **153**, 948 (2013).
- [15] J. Xu, S. N. Menon, R. Singh, N. B. Garnier, S. Sinha, and A. Pumir, The role of cellular coupling in the spontaneous generation of electrical activity in uterine tissue, *PLoS ONE* **10**, e0118443 (2015).
- [16] K. M. Myers and D. Elad, Biomechanics of the human uterus, *Wiley Interdiscip. Rev. Syst. Biol. Med.* **9**, e1388 (2017).
- [17] A. Karma, Physics of cardiac arrhythmogenesis, *Annu. Rev. Condens. Matter Phys.* **4**, 313 (2013).
- [18] S. Alonso, M. Bär, and B. Echebarria, Nonlinear physics of electrical wave propagation in the heart: A review, *Rep. Prog. Phys.* **79**, 096601 (2016).
- [19] T. Nagai and H. Honda, A dynamic cell model for the formation of epithelial tissues, *Philos. Mag. B* **81**, 699 (2001).
- [20] D. Bi, J. H. Lopez, J. M. Schwarz, and M. L. Manning, A density-independent rigidity transition in biological tissues, *Nat. Phys.* **11**, 1074 (2015).
- [21] D. Bi, X. Yang, M. C. Marchetti, and M. L. Manning, Motility-driven glass and jamming transitions in biological tissues, *Phys. Rev. X* **6**, 021011 (2016).

- [22] E. Tjhung and T. Kawasaki, Excitation of vibrational soft modes in disordered systems using active oscillation, *Soft Matter* **13**, 111 (2017).
- [23] E. Tjhung and L. Berthier, Discontinuous fluidization transition in time-correlated assemblies of actively deforming particles, *Phys. Rev. E* **96**, 050601(R) (2017).
- [24] C. Brito, E. Lerner, and M. Wyart, Theory for swap acceleration near the glass and jamming transitions for continuously polydisperse particles, *Phys. Rev. X* **8**, 031050 (2018).
- [25] N. Oyama, T. Kawasaki, H. Mizuno, and A. Ikeda, Glassy dynamics of a model of bacterial cytoplasm with metabolic activities, *Phys. Rev. Res.* **1**, 032038(R) (2019).
- [26] Y. Togashi, Modeling of nanomachine/micromachine crowds: Interplay between the internal state and surroundings, *J. Phys. Chem. B* **123**, 1481 (2019).
- [27] Y. Zhang and E. Fodor, Pulsating active matter, *Phys. Rev. Lett.* **131**, 238302 (2023).
- [28] D. R. Parisi, L. E. Wiebke, J. N. Mandl, and J. Textor, Flow rate resonance of actively deforming particles, *Sci. Rep.* **13**, 9455 (2023).
- [29] W. hua Liu, W. J. Zhu, and B. Q. Ai, Collective motion of pulsating active particles in confined structures, *New J. Phys.* **26**, 023017 (2024).
- [30] H. Ikeda and Y. Kuroda, Continuous symmetry breaking of low-dimensional systems driven by inhomogeneous oscillatory driving forces, *Phys. Rev. E* **110**, 024140 (2024).
- [31] Y. Kuramoto, *Chemical Oscillations, Waves, and Turbulence* (Springer, Berlin, 1984).
- [32] J. A. Acebrón, L. L. Bonilla, C. J. Pérez Vicente, F. Ritort, and R. Spigler, The Kuramoto model: A simple paradigm for synchronization phenomena, *Rev. Mod. Phys.* **77**, 137 (2005).
- [33] W. D. Piñeros and E. Fodor, Biased ensembles of pulsating active matter, *Phys. Rev. Lett.* **134**, 038301 (2025).
- [34] See Supplemental Material at <http://link.aps.org/supplemental/10.1103/PhysRevE.111.L053401> for details of the analytical calculations and numerical simulations, as well as two videos, which also includes Refs. [65–67].
- [35] I. S. Aranson and L. Kramer, The world of the complex Ginzburg-Landau equation, *Rev. Mod. Phys.* **74**, 99 (2002).
- [36] *In Mathematical Biology I: An Introduction* edited by J. D. Murray (Springer, New York, 2002).
- [37] J. D. Murray, *Mathematical Biology II: Spatial models and biomedical applications* (Springer, New York, 2003).
- [38] G. Ódor, Universality classes in nonequilibrium lattice systems, *Rev. Mod. Phys.* **76**, 663 (2004).
- [39] A. G. Thompson, J. Tailleur, M. E. Cates, and R. A. Blythe, Lattice models of nonequilibrium bacterial dynamics, *J. Stat. Mech.* (2011) P02029.
- [40] C. Maes and S. Shlosman, Rotating states in driven clock- and XY-models, *J. Stat. Phys.* **144**, 1238 (2011).
- [41] A. P. Solon and J. Tailleur, Revisiting the flocking transition using active spins, *Phys. Rev. Lett.* **111**, 078101 (2013).
- [42] A. P. Solon and J. Tailleur, Flocking with discrete symmetry: The two-dimensional active Ising model, *Phys. Rev. E* **92**, 042119 (2015).
- [43] A. Manacorda and A. Puglisi, Lattice model to derive the fluctuating hydrodynamics of active particles with inertia, *Phys. Rev. Lett.* **119**, 208003 (2017).
- [44] A. Manacorda, *Lattice Models for Fluctuating Hydrodynamics in Granular and Active Matter* (Springer, Berlin, 2018).
- [45] M. Kourbane-Houssene, C. Erignoux, T. Bodineau, and J. Tailleur, Exact hydrodynamic description of active lattice gases, *Phys. Rev. Lett.* **120**, 268003 (2018).
- [46] A. Solon, H. Chaté, J. Toner, and J. Tailleur, Susceptibility of polar flocks to spatial anisotropy, *Phys. Rev. Lett.* **128**, 208004 (2022).
- [47] F. Y. Wu, The Potts model, *Rev. Mod. Phys.* **54**, 235 (1982).
- [48] T. Herpich, J. Thingna, and M. Esposito, Collective power: Minimal model for thermodynamics of nonequilibrium phase transitions, *Phys. Rev. X* **8**, 031056 (2018).
- [49] T. Herpich and M. Esposito, Universality in driven Potts models, *Phys. Rev. E* **99**, 022135 (2019).
- [50] E. Panteley, A. Loria, and A. E. Ati, On the stability and robustness of Stuart-Landau oscillators, *IFAC-PapersOnLine* **48**, 645 (2015).
- [51] T. Reichenbach, M. Mobilia, and E. Frey, Mobility promotes and jeopardizes biodiversity in rock-paper-scissors games, *Nature (London)* **448**, 1046 (2007).
- [52] T. Reichenbach, M. Mobilia, and E. Frey, Self-organization of mobile populations in cyclic competition, *J. Theor. Biol.* **254**, 368 (2008).
- [53] S. Shankar, A. Souslov, M. J. Bowick, M. C. Marchetti, and V. Vitelli, Topological active matter, *Nat. Rev. Phys.* **4**, 380 (2022).
- [54] B. Mahault, E. Tang, and R. Golestanian, A topological fluctuation theorem, *Nat. Commun.* **13**, 3036 (2022).
- [55] Y. Avni, M. Fruchart, D. Martin, D. Seara, and V. Vitelli, Non-reciprocal Ising model, *Phys. Rev. Lett.* **134**, 117103 (2025).
- [56] Y. Avni, M. Fruchart, D. Martin, D. Seara, and V. Vitelli, Dynamical phase transitions in the nonreciprocal Ising model, *Phys. Rev. E* **111**, 034124 (2025).
- [57] H. Noguchi, F. van Wijland, and J.-B. Fournier, Cycling and spiral-wave modes in an active cyclic Potts model, *J. Chem. Phys.* **161**, 025101 (2024).
- [58] H. Noguchi and J.-B. Fournier, Spatiotemporal patterns in the active cyclic Potts model, *New J. Phys.* **26**, 093043 (2024).
- [59] T. Banerjee, T. Desaleux, J. Ranft, and É. Fodor, Hydrodynamics of pulsating active liquids, [arXiv:2407.19955](https://arxiv.org/abs/2407.19955).
- [60] T. Agranov, R. L. Jack, M. E. Cates, and É. Fodor, Thermodynamically consistent flocking: From discontinuous to continuous transitions, *New J. Phys.* **26**, 063006 (2024).
- [61] J. Meibohm and M. Esposito, Small-amplitude synchronization in driven Potts models, *Phys. Rev. E* **110**, 044114 (2024).
- [62] J. Meibohm and M. Esposito, Minimum-dissipation principle for synchronized stochastic oscillators far from equilibrium, *Phys. Rev. E* **110**, L042102 (2024).
- [63] F. Avanzini, T. Aslyamov, E. Fodor, and M. Esposito, Nonequilibrium thermodynamics of non-ideal reaction-diffusion systems: Implications for active self-organization, *J. Chem. Phys.* **161**, 174108 (2024).
- [64] A. Manacorda, Species interconversion of deformable particles yields transient phase separation data set, 2025, doi:[10.17605/OSF.IO/DEV23](https://doi.org/10.17605/OSF.IO/DEV23).
- [65] O. Tange, GNU parallel—The command-line power tool, *USENIX Mag.* **36**, 42 (2011).
- [66] C. W. Gardiner, *Stochastic Methods: A Handbook for the Natural and Social Sciences* (Springer, Berlin, 2009), Vol. 4.
- [67] W. Liu and U. C. Täuber, Nucleation of spatiotemporal structures from defect turbulence in the two-dimensional complex Ginzburg-Landau equation, *Phys. Rev. E* **100**, 052210 (2019).